

# The Panchromatic Hubble Andromeda Treasury. Progression of Large-Scale Star Formation across Space and Time in M 31

Dimitrios A. Gouliermis, Lori C. Beerman, Luciana Bianchi, Julianne J. Dalcanton, Andrew E. Dolphin, Morgan Fouesneau, Karl D. Gordon, Puragra Guhathakurta, Jason Kalirai, Dustin Lang, Anil Seth, Evan Skillman, Daniel R. Weisz, and Benjamin F. Williams

**Abstract** We investigate the clustering of early-type stars younger than 300 Myr on galactic scales in M 31. Based on the stellar photometric catalogs of the Panchromatic Hubble Andromeda Treasury program that also provides stellar parameters derived from the individual energy distributions, our analysis focused on the young stars in three star-forming regions, located at galactocentric distances of about 5, 10, and 15 kpc, corresponding to the inner spiral arms, the ring structure, and the outer arm, respectively. We apply the two-point correlation function to our selected sample to investigate the clustering behavior of these stars across different time- and length-scales. We find that young stellar structure survives across the whole extent of M 31 longer than 300 Myr. Stellar distribution in all regions appears to be self-similar, with younger stars being systematically more strongly clustered than the older, which are more dispersed. The observed clustering is interpreted as being induced by turbulence, the driving source for which is probably gravitational instabilities driven by the spiral arms, which are stronger closer to the galactic centre.

## 1 Introduction

Stars are born in groups (Lada & Lada, 2003) of various sizes and with various degrees of gravitational self-binding (Elmegreen et al., 2000). Observed length-scales of star formation range from few 100-pc, typical for loose stellar complexes, to few 10-pc, characteristic of unbound stellar aggregates and OB associations, and finally down to few pc, indicative of more compact young star clusters. All these types of stellar clusterings are not independent from each other and instead, they

---

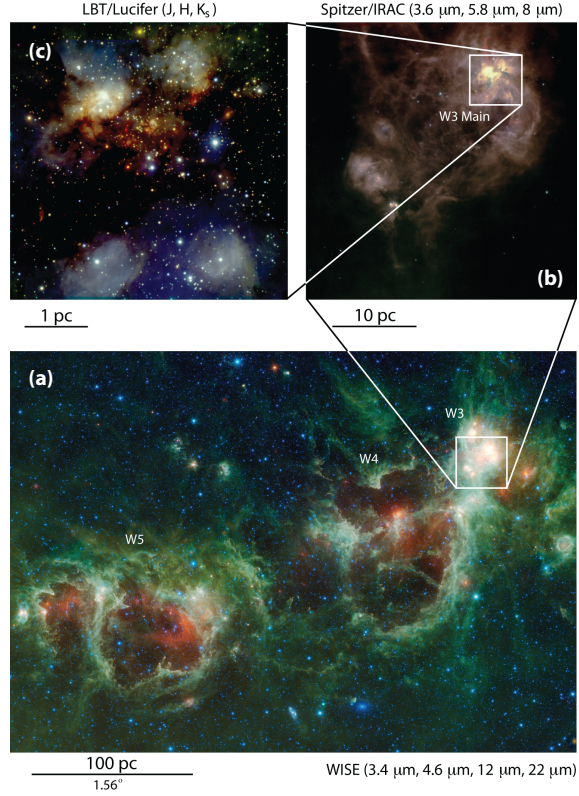
Dimitrios A. Gouliermis

University of Heidelberg, Centre for Astronomy, Institute for Theoretical Astrophysics, Albert-Ueberle-Str. 2, 69120 Heidelberg, Germany;

Max Planck Institute for Astronomy, Königstuhl 17, 69117 Heidelberg, Germany

email: dgoulierm@googlemail.com; dgoulier@mpia.de

**Fig. 1** Hierarchy in the ISM and stellar clustering in the general area of W3 complex. (a) On 100 pc-scale, the nebular structures W4 and W5 are shown in the mid-IR image from NASA/WISE, which covers the general region of the OB association Cas OB6. (b) On 10 pc-scale, the star-forming region W3, considered as part of W4, is shown from NASA/Spitzer images, with the active star-forming region W3 Main showing bright PAH emission at  $8\mu\text{m}$ . (c) Finally, on the 1 pc-scale high-resolution near-IR images from LUCI camera on the LBT reveal the embedded star-forming cluster of W3 Main (Bik et al., 2012, 2014). WISE image credit: NASA/JPL-Caltech/WISE Team.



are structured into a hierarchical fashion (Elmegreen 2011), similar to that of the interstellar matter (ISM). Giant molecular clouds are indeed hierarchical structures (Elmegreen & Falgarone, 1996; Stutzki et al., 1998), indicating that scale-free processes determine their global morphology, turbulence being considered the dominant (Elmegreen & Scalo, 2004; Mac Low & Klessen, 2004). It stands to reason that mechanisms regulating star formation (McKee & Ostriker, 2007) consequently shape stellar structures, which then build up in a hierarchical fashion, due to the self-similar nature of turbulent cascade (e.g., Klessen & Burkert, 2000). This structuring behavior is exemplified in Fig. 1 for the Galactic star-forming complex W3/4/5.

The formation of stars proceeds hierarchically also in time. The duration of star formation tends to increase with the size of the region as the crossing time for turbulent motions (Efremov & Elmegreen, 1998). Small regions form stars quickly and large regions, which contain the small ones, form stars over a longer period. This relation between length- and time-scale underscores the perception that both, cloud and stellar structures, come from interstellar gas turbulence and suggests that star formation in a molecular cloud is finished within only few turbulent crossing times (e.g., Ballesteros-Paredes et al., 1999; Elmegreen, 2000; Hartmann et al., 2001).

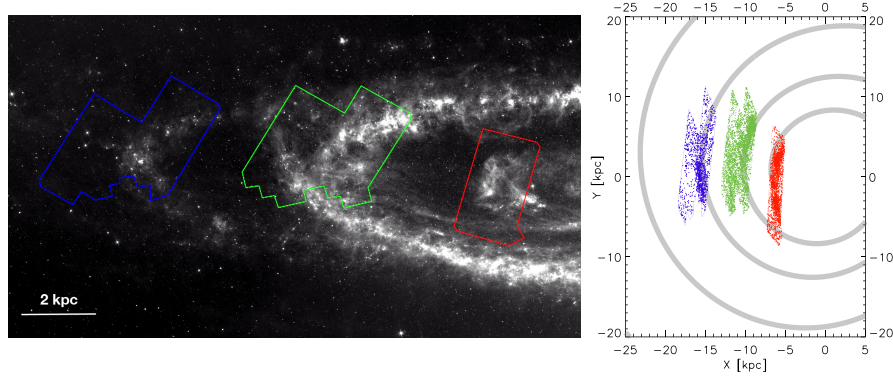


**Fig. 2** Footprints of the selected regions on the *Spitzer*  $8\mu\text{m}$  image of M 31 (left panel), and coverage of the selected regions in respect to the Andromeda disk corrected for the inclination of the galaxy, shown face-on (right panel), in respect to the spiral arms in accordance to Arp (1964). Area 9 (red) covers the northeastern turn-over of the inner spiral arm at  $\sim 5$  kpc from the centre, and area 15 (green) that of the second arm on the 10 kpc star-forming ring of Andromeda. Area 21 (blue) located at distance  $\sim 15$  kpc from the centre, includes various star-forming regions at the outskirts of M 31.

While this picture of clustered star formation explains the formation of young stellar assemblies across different scales, the relation between ISM structure and stellar clustering is not well understood. In addition, apart from star formation, environmental conditions (local feedback, galactic dynamics, etc) influence the morphology of stellar clustering, and the observed variety of stellar systems in size, shape, and compactness. Dissentangling the relative importance of the heredity of star formation to the stellar clustering (“nature”) in comparison to the environmental influence on its morphology and survival (“nurture”) plays, thus, an important role to our understanding of clustered star formation.

We present our investigation of stellar structures formation over galactic scales from the census of bright blue stars, distributed over the typical length-scale of spiral arms. Our dataset is observed with the most complete stellar survey ever performed of M 31, obtained by the *Panchromatic Hubble Space Telescope Andromeda Galaxy Treasury* program<sup>1</sup>. We describe our analysis and present first results on the clustering behaviour of young stars up to ages of  $\sim 300$  Myr in this galaxy.

## 2 Observational material

The *Panchromatic Hubble Space Telescope Andromeda Treasury* (PHAT) program (Dalcanton et al., 2012) provides deep coverage of 1/3 of M 31 galaxy in six filters with *HST*. The survey spans the north east quadrant of the galaxy, continuously imaging from the nucleus to the last obvious regions of star formation visible with

<sup>1</sup> <http://www.astro.washington.edu/groups/phat/Home.html>

GALEX (e.g., Thilker et al., 2005). This part of M 31 is selected because of its lowest internal extinction, the highest intensity regions of unobscured star formation, and the least contamination from M 32. Imaging is performed blue-ward of  $4000\text{\AA}$ , in filters F275W and F336W with the WFC3 camera, in the optical F475W and F814W filters with ACS/WFC, and in the near-IR, in the WFC3 filters F110W and F160W (Williams et al., 2014). This wide panchromatic coverage baseline allows us to confidently estimate stellar effective temperatures, masses, ages and reddenings through a self-consistent Bayesian Spectral Energy Distribution (SED) fitting technique (Gordon et al., in prep), and identify specific features on the color-magnitude diagrams (CMDs) for hot and cool stars for a wide range of extinctions. The homogeneity of the stellar photometric catalogs produced by PHAT over a wide spatial coverage provides the unique opportunity to address the clustering behavior of star formation at length-scales of few kpc, corresponding to spiral arms, down to the few pc scale, where individual star clusters reside (Johnson et al., 2012; Fouesneau et al., 2014; Simones et al., 2014).

Observations of the PHAT survey were performed in  $3 \times 6$  mosaics of 18 parallel ACS and WFC3 pointings. Each mosaic builds a so-called ‘brick’, roughly corresponding to regions of  $1.5 \times 3$  kpc at the distance of M 31. In total, 23 such bricks tile the complete survey area. The regions of interest in our study are covered by few such bricks, all including portions of the star-forming spiral arms and 10-kpc ring of Andromeda (Fig. 2). We name each area after the identification number of its first brick, e.g., areas 9, 15 and 21. Area 9 covers only one brick, while areas 15 and 21 cover somewhat more than two adjacent bricks. These (apart from a brick that covers part of the bulge) are the only areas for which preliminary stellar parameters are available through our SED fitting technique. We distinguish the bright hot stars with the best-fit values in each area, based on three selection criteria:

1. Stars with  $T_{\text{eff}} \geq 10,000$  K, i.e., spectral type earlier than  $\sim A0V$ .
2. Stars detected in at least three of the bluest filters, i.e., in F275W (NUV), F336W (U), and F475W (B).
3. Stars with equivalent U-band magnitude  $m_{336} \leq 25.25$ .

With these criteria, we ensure to select the brightest young stars with  $L \gtrsim 80 L_{\odot}$ , and also the most accurate determinations of physical parameters based on the preliminary assumed stellar models.

### 3 Evolution of young stellar structure in M 31

#### 3.1 The two-point correlation function

The spatial distribution of the early-type stars in the selected areas is characterized in terms of the two-point correlation function (TPCF). Originally introduced for measuring cosmological structure (e.g., Peebles, 1980), the TPCF is a robust



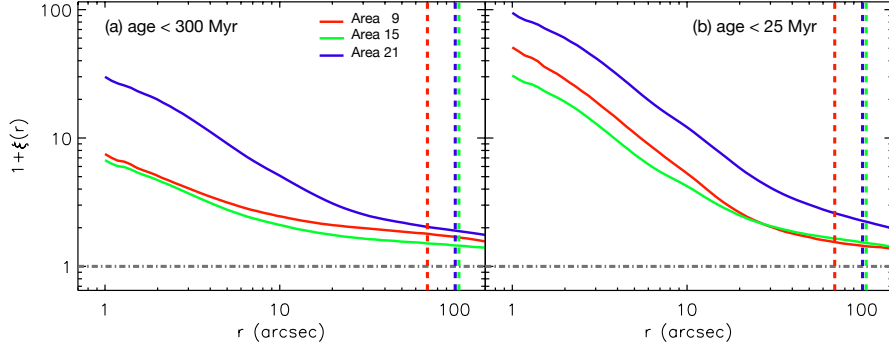


**Fig. 3** The TPCF of the three areas of interest constructed for stars in two different age ranges, i.e., the complete samples with stellar ages up to  $\sim 300$  Myr and a subsample of stars with ages up to 25 Myr. All TPCFs behave as power-laws up to specific separations, beyond which the TPCF index evidently changes. Vertical lines, coloured accordingly, correspond to the limiting separations beyond which the effects of the limited field-of-view become dominant, and thus TPCF measurements are not trustful (see, e.g., Gouliermis et al., 2014).

measurement of the degree of clustering in a sample of sources. Based on the original estimator by Peebles & Hauser (1974) the TPCF is estimated by counting the pairs of sources with different separations  $r$ . This function is defined as (see, e.g., Scheepmaker et al., 2009):

$$1 + \xi(r) = \frac{1}{\bar{n}N} \sum_{i=1}^N n_i(r), \quad (1)$$

which measures the surface density enhancement  $n_i(r)$  within radius  $r$  from star  $i$  with respect to the global average surface density  $\bar{n}$  of the total sample of  $N$  stars. For a fractal distribution the TPCF yields a power-law dependency with radius of the form  $1 + \xi(r) \propto r^\eta$ . By definition, the total number of stars  $N_r$  within an aperture of radius  $r$  will be then increasing as  $N_r \propto r^\eta \cdot r^2 = r^{\eta+2}$ . The power-law index  $\eta$  is thus related to the (two-dimensional) fractal dimension,  $D_2$ , of the (projected) distribution as  $D_2 = \eta + 2$  (Mandelbrot, 1983).

This TPCF formalism allows for the direct interpretation of the absolute value of  $1 + \xi(r)$ , without any comparison with a reference random distribution (as, e.g., proposed by Gomez et al., 1993), because for a random (Poisson) stellar distribution the value of the TPCF is always  $1 + \xi(r) = 1$ , independent of  $r$ . For truly clustered distributions the value of the TPCF is a measurement of the clustering degree of the stars, and is always  $> 1$ ; higher value at a given separation, stands for higher degree of clustering in the sample (for a complete description see Gouliermis et al., 2014, and references therein). The behaviour of the TPCF is illustrated by the examples given in Fig. 3, where the TPCFs of the three areas for the complete sample of stars with ages up to  $\sim 300$  Myr and stars with ages up to  $\sim 25$  Myr, are shown.

The log-log plots of Fig. 3 show that all TPCFs have broken power-law shape. We determine the index  $\eta$  of each part of the TPCF by applying a Levenberg–Marquard

nonlinear least square minimization fit (Levenberg, 1944; Marquardt, 1963). The fitting function has the form:

$$\log(1 + \xi(r)) = \begin{cases} \alpha + \beta \cdot \log(r) & \text{for } \log(r) < \delta \\ \alpha + (\beta - \gamma) \cdot \delta + \gamma \cdot \log(r) & \text{for } \log(r) > \delta \end{cases} \quad (2)$$

where  $\beta$  and  $\gamma$  are the power-law slopes and  $\delta$  is the logarithm of the position of the separation break along the abscissa,  $S_{\text{break}}$ , where the TPCF index changes. Both slopes and the separation break are free parameters in our fit.

From the comparison of the TPCFs of Fig. 3 we derive two interesting results. First, the younger stars (age  $\lesssim 25$  Myr) show a more fractal, i.e., clumpy, clustering than stars in the whole sample (age  $\lesssim 300$  Myr). This is demonstrated by both the higher values of  $1 + \xi$  at small separations and the steeper slopes of their TPCFs (the latter only for areas 9 and 15). Second, while the TPCF index of areas 9 and 15 changes significantly, becoming steeper for the younger sample, that of area 21 remains unchanged between the two samples. This indicates that older populations (up to  $\sim 300$  Myr) in areas 9 and 15 have higher filling factors (flatter TPCF slopes) than those in area 21. Considering that the latter is the most remote area, away from the centre of M 31, we can only assume that the more dispersed distribution of older stars in areas 9 and 15 is due to the dynamics of the galaxy. We investigate in more detail the evolution of the TPCF with stellar age in the following sections.

### 3.2 Evolution of the TPCF with time

We construct the TPCF of the young stellar samples in the three areas of interest for stars of different ages. We divide each sample to several subsamples of stars, according to the best-fit ages assigned to each star with the SED-fitting. These ages are constrained by the stellar evolution models (Girardi et al., 2010) and atmosphere templates (Castelli & Kurucz, 2004) preliminary used in our technique. Therefore, we select our subsamples of stars according to their effective temperatures, which are somewhat better-constrained by the SED fitting, and are clear indicators of the stellar evolutionary stage. In order for our analysis to be performed in samples of equivalent statistical significance (i.e., not being affected by different number statistics) we divided each stellar catalog into  $T_{\text{eff}}$ -determined subsamples, containing the same number of stars, corresponding to  $\sim 10\%$  of the total. We divided thus each stellar catalog into nine (in the case of area 9 into ten) subsamples that contain almost identical number of stars at different evolutionary stages. This number is  $\sim 5,000$  in areas 9 and 21 and  $\sim 10,000$  in area 15. An example of the subsamples and the derived TPCF parameters for area 15 is shown in Table 1.

We determine the TPCF index  $\eta$  for both small and large separations, as well as the separation  $S_{\text{break}}$  where  $\eta$  changes, for each subsample by applying again a Levenberg–Marquard nonlinear least square minimization fit. The results are given

**Table 1** Selected stellar subsamples and derived TPCF parameters for area 15.

$\langle \log T_{\text{eff}} \rangle^a$	$\langle \text{age} \rangle^b$ (Myr)	age limits <sup>c</sup> (Myr)	$\bar{n}^d$ ( $10^{-4}$ $\text{pc}^{-2}$ )	$D^e$ (small separations)	$D$ (large separations)	Separation break <sup>f</sup> (pc)
4.38	$9 \pm 7$	0.2 – 29.0	2.7	$0.955 \pm 0.004$	$1.583 \pm 0.012$	$83.37 \pm 3.83$
4.26	$21 \pm 15$	1.0 – 52.7	3.3	$1.485 \pm 0.069$	$1.835 \pm 0.016$	$51.40 \pm 4.71$
4.21	$34 \pm 24$	0.9 – 75.4	3.5	$1.626 \pm 0.185$	$1.883 \pm 0.020$	$43.70 \pm 7.27$
4.17	$51 \pm 30$	1.0 – 84.1	3.3	$1.646 \pm 0.249$	$1.904 \pm 0.028$	$46.37 \pm 9.14$
4.14	$70 \pm 37$	3.8 – 109.0	2.7	$1.624 \pm 0.218$	$1.904 \pm 0.026$	$47.61 \pm 7.85$
4.11	$104 \pm 40$	7.7 – 151.0	2.2	$1.729 \pm 0.361$	$1.925 \pm 0.024$	$39.79 \pm 16.49$
4.08	$145 \pm 44$	10.2 – 188.0	2.6	$1.668 \pm 0.290$	$1.904 \pm 0.021$	$36.28 \pm 10.70$
4.04	$193 \pm 51$	11.0 – 242.0	2.5	$1.628 \pm 0.209$	$1.888 \pm 0.020$	$37.58 \pm 7.69$
4.01	$252 \pm 63$	13.1 – 318.0	2.6	$1.601 \pm 0.137$	$1.882 \pm 0.022$	$50.90 \pm 6.06$

<sup>a</sup> Average logarithmic effective temperature of stars in the subsample.<sup>b</sup> Average age of stars in the subsample.<sup>c</sup> Age limits of stars in the subsample.<sup>d</sup> Mean stellar surface density.<sup>e</sup> Two-dimensional fractal dimension derived from the TPCF index  $\eta$  as  $D = \eta + 2$ .<sup>f</sup> Separation limit, where the TPCF shows a significant change in its slope  $\eta$ .

in Fig. 4, where we show the relation of index  $\eta$  (and the derived  $D_2$ ) to the average age of the corresponding stellar subsample for small ( $r \leq S_{\text{break}}$ ; top panel) and large ( $r \geq S_{\text{break}}$ ; middle panel) separations.

For small separations the plots of  $\eta$  (or  $D_2$ ) versus stellar age show that there is a clear time evolution of the TPCF, with  $D_2$  being smaller at younger ages, and becoming larger for older ages. In all areas  $D_2$  starts with values  $\lesssim 1$  at the smaller age bin of  $\langle \text{age} \rangle \sim 9$  Myr, and increases almost monotonically to a value of  $\sim 1.6$  at  $\langle \text{age} \rangle \sim 75$  Myr for area 9 and 35 Myr for area 15 (see also Table 1), and to  $\sim 1.4$  at  $\langle \text{age} \rangle \sim 45$  Myr for area 21. It is worth noting that while for older stars in areas 9 and 15 the TPCF slope ‘stabilizes’ at almost constant value through the whole remaining age extent, in area 21 it drops again to the value of  $D_2 \sim 1$ . For separations  $r \geq S_{\text{break}}$  (Fig. 4, middle panel) the TPCF shows no important evolution with stellar age, having a value of  $D_2 \sim 1.85 \pm 0.02$  (area 9),  $\sim 1.85 \pm 0.11$  (area 15), and  $\sim 1.79 \pm 0.07$  (area 21). While this value for area 21 is somewhat smaller than those in areas 9 and 15, all values are high, close to the geometrical (projected) dimension, and thus consistent with almost uniform (non-clustered) stellar distributions. Interestingly, we observe from the bottom panels of Fig. 4, that the limit of the fractal regime,  $S_{\text{break}}$ , seems to also evolve with stellar age.

## 4 Concluding Remarks and Summary

The value  $D_2 \lesssim 1$  found for the youngest stars at separations  $r \leq S_{\text{break}}$  indicates that star formation is clumpy, forming well-clustered (highly fractal) stellar distributions. This clustering behavior becomes somewhat scattered (larger  $D_2$ ) for older stars, sta-

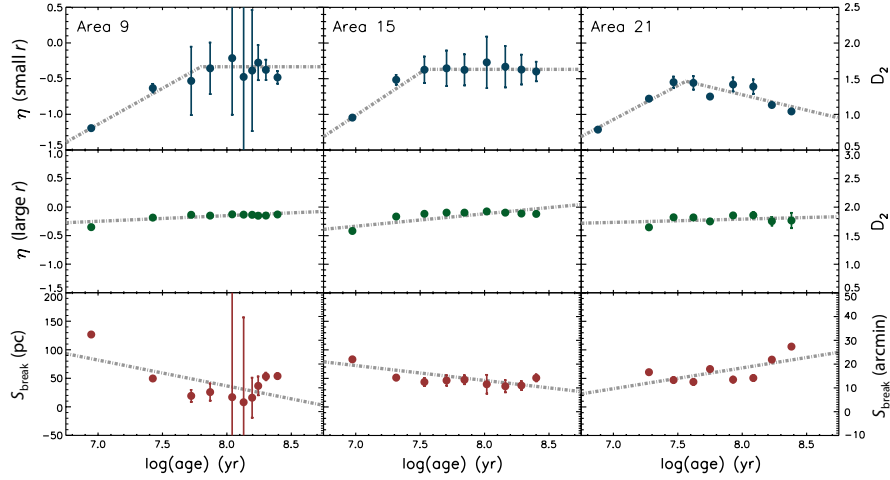


**Fig. 4** Evolution of the TPCF as a function of stellar age for the three areas of interest. *Top panel:* Relation of the TPCF index  $\eta$  (or the equivalent fractal dimension  $D_2$ , given on the right ordinate) to average stellar age for small separations (smaller than the length  $S_{\text{break}}$  where the TPCF slope changes). *Middle panel:* The same relation for large separations, i.e.,  $r \geq S_{\text{break}}$ . *Bottom panel:* Relation of  $S_{\text{break}}$  to average stellar age for each subsample. The grey dash-dotted lines are linear fits to the data. The TPCF of stars in the youngest age range of area 21 is a single power-law, and therefore there is no measurement for  $D_2$  at large separations and  $S_{\text{break}}$  for this age.

bilizing at  $D_2 \sim 1.4 - 1.6$ , up to  $\sim 300$  Myr. This fractal dimension, however, is still characteristic of self-similarity, indicating that while stellar clustering does evolve with time, the original structure in M 31 persists over more than  $\sim 300$  Myr. This time-scale is in agreement with the lower limits placed for structure survival in dwarf galaxies (Bastian et al., 2011). Values of  $D_2 \sim 1.5$ , measured in the distributions of size and luminosity of star-forming regions in the spiral galaxy NGC 628, and across the whole extend of star-forming galaxies of various types, are interpreted as indication of hierarchy induced by turbulence (Elmegreen et al., 2006; Elmegreen et al., 2014). Similarly, we conclude that the observed fractal dimensions in all three areas may be driven by turbulent processes on galactic scales.

The change of the TPCF index at  $r \simeq S_{\text{break}}$  and the stability of  $D_2$  to an almost constant value for separations  $r > S_{\text{break}}$  suggests that possibly there is a maximum length-scale up to which stars sustain their clustering pattern, i.e., up to which their structures survive. Moreover, the apparent dependence of  $S_{\text{break}}$  to stellar age implies that this scale differs between stars at different evolutionary stages. Although the physical meaning of this break is not yet understood, its presence might be related to the scale of the galactic disk. For example, a break in the power spectra of ISM emission in the Large Magellanic Cloud is interpreted as due to the line-of-sight thickness of the galactic disk (Block et al., 2010). Indeed, in spiral galaxies stars tend to group up to scales comparable to the disk scale height, and larger structures become spiral-like (flocculent) because of their longer dynamical time-scales in comparison to the shear time (see, e.g., Elmegreen, 2011).

*Under these circumstances, with the use of the TPCF, we not only determine the time-scale for structure survival, but we may also specify the upper length-scale limit across the galactic disk where structure survives, before it ‘dis-solves’ in it.*

The observed difference in the behavior of the TPCF from one area to other, suggests a possible dependence of the clustering behavior of stars to the position of the areas across the disk of M 31, and thus the dynamical influence of the galaxy. Area 9 coincides with the first arm at distance  $\sim 5$  kpc, area 15 is located at the 10 kpc star-forming ring, and the more remote area 21 at a distance  $\sim 15$  kpc away from the galactic centre (see Fig. 2, right panel). Area 9, being closer to the centre, experiences stronger gravitational instabilities and possible disruption by the galactic potential. This is portrayed by the TPCF (at small separations) and  $S_{\text{break}}$  variabilities, which are seen in Fig. 4 only for area 9, and not for areas 15 and 21.

Considering the rotation of the galaxy (e.g., Sofue & Rubin, 2001), based on their positions, all three areas have rotational velocities quite similar to each other varying between  $236 \text{ km s}^{-1}$  at  $\sim 5$  kpc,  $260 \text{ km s}^{-1}$  at  $\sim 10$  kpc, and  $251 \text{ km s}^{-1}$  at  $\sim 15$  kpc (see, e.g., Table 1 in Carignan et al., 2006). While all areas have similar velocities, being at different distances from the galactic centre, perform a complete orbit at different time-scales, the closest being fastest. As a consequence, the oldest stars in our samples, of  $\sim 300$  Myr, have performed thus far 10% of an orbit in area 9, 6% in area 15 and 4% in area 21. This suggests that these stars have experienced different degrees of streaming motions driven by the spiral arms, which scatter stars as they shear by (e.g., Elmegreen & Struck, 2013), with those in area 21 being less disrupted.

Based on the discussion above, the findings of this study can be summarized to the following points:

1. Stellar clustering occurs at length-scales that depend on both stellar age and position on the disk.
2. Star formation produces clumpy structures of young stars, on which galactic dynamics influence over time subsequent clustering processes or substructures.
3. Young stellar structures survive across the whole extend of M 31 for at least  $\sim 300$  Myr.
4. The distribution of young stars evolves as a function of stellar age, but remains fractal with  $D_2 \sim 1.4 - 1.6$  up to this age limit.
5. The observed self-similarity in the stellar distribution is probably induced by large-scale turbulence.
6. Stars in the outer parts away from the galactic centre experience less disruption driven by the gravity of spiral arms.

**Acknowledgements** Based on observations made with the NASA/ESA *Hubble Space Telescope*, obtained from the data archive at the Space Telescope Science Institute (STScI). STScI is operated by the Association of Universities for Research in Astronomy, Inc. under NASA contract

NAS 5-26555. D.A.G. acknowledges support by the German Research Foundation through grant GO 1659/3-1. I also acknowledge very useful discussions with Bruce Elmegreen, Ralf Klessen, Sacha Hony and Lukas Konstandin, which helped improve this manuscript. Finally, I would like to thank the organizers for a very interesting meeting in a wonderful location, and wish to our honourees and their beloved all the best for good health and happiness!

## References

- Arp, H. 1964, *ApJ*, 139, 1045
- Ballesteros-Paredes, J., Hartmann, L., & Vázquez-Semadeni, E. 1999, *ApJ*, 527, 285
- Bastian, N., Weisz, D. R., Skillman, E. D., et al. 2011, *MNRAS*, 412, 1539
- Bik, A., Henning, T., Stolte, A., et al. 2012, *ApJ* 744, 87
- Bik, A., Stolte, A., Gennaro, M., et al. 2014, *A&A*, 561, A12
- Block, D. L., Puerari, I., Elmegreen, B. G., & Bournaud, F. 2010, *ApJL*, 718, L1
- Carignan, C., Chemin, L., Huchtmeier, W. K., & Lockman, F. J. 2006, *ApJL*, 641, L109
- Castelli, F., & Kurucz, R. L. 2004, *A&A*, 419, 725
- Dalcanton, J. J., Williams, B. F., Lang, D., et al. 2012, *ApJS*, 200, 18
- Efremov, Y. N., & Elmegreen, B. G. 1998, *MNRAS*, 299, 588
- Elmegreen, B. G. 2000, *ApJ*, 530, 277
- Elmegreen, B. G. 2011, *EAS Publications Series*, 51, 31
- Elmegreen, B. G. & Falgarone, E. 1996, *ApJ*, 471, 816
- Elmegreen, B. G., & Scalo, J. 2004, *ARA&A*, 42, 211
- Elmegreen, B. G., Efremov, Y., Pudritz, R. E., et al. 2000, *Protostars and Planets IV*, 179
- Elmegreen, B. G., Elmegreen, D. M., Chandar, R., et al. 2006, *ApJ*, 644, 879
- Elmegreen, B. G., & Struck, C. 2013, *ApJL*, 775, L35
- Elmegreen, D. M., Elmegreen, B. G., Adamo, A., et al. 2014, *ApJL*, 787, L15
- Fouesneau, M., Johnson, L. C., Weisz, D. R., et al. 2014, *ApJ*, 786, 117
- Girardi, L., Williams, B. F., Gilbert, K. M., et al. 2010, *ApJ*, 724, 1030
- Gomez, M., Hartmann, L., Kenyon, S. J., & Hewett, R. 1993, *AJ*, 105, 1927
- Gouliermis, D. A., Hony, S., & Klessen, R. S. 2014, *MNRAS*, 439, 3775
- Johnson, L. C., Seth, A. C., Dalcanton, J. J., et al. 2012, *ApJ*, 752, 95
- Hartmann, L., Ballesteros-Paredes, J., & Bergin, E. A. 2001, *ApJ*, 562, 852
- Klessen, R. S., & Burkert, A. 2000, *ApJS*, 128, 287
- Lada, C. J., & Lada, E. A. 2003, *ARA&A*, 41, 57
- Levenberg, K. 1944, *Q. Appl. Math.*, 2, 164
- Mac Low, M.-M., & Klessen, R. S. 2004, *Reviews of Modern Physics*, 76, 125
- Mandelbrot, B. B. 1983, *The fractal geometry of nature* (Freeman, San Francisco)
- Marquardt, D. 1963, *SIAM J. Appl. Math.*, 11, 431
- McKee, C. F., & Ostriker, E. C. 2007, *ARA&A*, 45, 565
- Peebles, P. J. E. 1980, *The Large-Scale Structure of the Universe*. Princeton Univ. Press
- Peebles, P. J. E., & Hauser, M. G. 1974, *ApJSS*, 28, 19
- Scheepmaker, R. A., Lamers, H. J. G. L. M., Anders, P., & Larsen, S. S. 2009, *A&A*, 494, 81
- Simones, J. E., Weisz, D. R., Skillman, E. D., et al. 2014, *ApJ*, 788, 12
- Sofue, Y., & Rubin, V. 2001, *ARA&A*, 39, 137
- Stutzki J., Bensch F., Heithausen A., Ossenkopf V., & Zielinsky M. 1998, *A&A* 336, 697
- Thilker, D. A., Hoopes, C. G., Bianchi, L., et al. 2005, *ApJL*, 619, L67
- Williams, B. F., Dalcanton, J. J., Lang, D., et al. 2014, *ApJ*, submitted